University of Texas Rio Grande Valley
ScholarWorks @ UTRGV

Theses and Dissertations

5-2021

OPA1 Modulation of Mitochondrial Dynamics in AC16 Cardiomyocytes

Patrick De La Torre Schutz
The University of Texas Rio Grande Valley

Follow this and additional works at: https://scholarworks.utrgv.edu/etd

 Part of the Biology Commons

Recommended Citation

De La Torre Schutz, Patrick, "OPA1 Modulation of Mitochondrial Dynamics in AC16 Cardiomyocytes" (2021). *Theses and Dissertations*. 852.
https://scholarworks.utrgv.edu/etd/852

This Thesis is brought to you for free and open access by ScholarWorks @ UTRGV. It has been accepted for inclusion in Theses and Dissertations by an authorized administrator of ScholarWorks @ UTRGV. For more information, please contact justin.white@utrgv.edu, william.flores01@utrgv.edu.

OPA1 MODULATION OF MITOCHONDRIAL DYNAMICS IN AC16 CARDIOMYOCYTES

A Thesis

by

PATRICK DE LA TORRE SCHUTZ

Submitted to the Graduate College of
The University of Texas Rio Grande Valley
In partial fulfillment of the requirements for the degree of

MASTER OF SCIENCE

May 2021

Major Subject: Biology

OPA1 MODULATION OF MITOCHONDRIAL DYNAMICS IN AC16 CARDIOMYOCYTES

A Thesis
by
PATRICK DE LA TORRE SCHUTZ

COMMITTEE MEMBERS

Dr. Robert Gilkerson
Chair of Committee

Dr. Megan Keniry
Committee Member

Dr. Nirakar Sahoo
Committee Member

May 2021

Copyright 2021 Patrick De La Torre Schutz
All Rights Reserved

ABSTRACT

De La Torre Schutz, Patrick, OPA1 modulation of mitochondrial dynamics in AC16 cardiomyocytes. Master of Science (MS), May, 2021, 20 pp., 4 figures, 12 references, 10 titles.

This thesis explores mitochondrial dynamics in the AC16 cardiomyocytes. Mitochondria are capable of fission and fusion, controlled by specific proteins that respond to cell stress. The transmembrane potential($\Delta\psi_m$) of the mitochondria is responsible for both bioenergetic functions and regulating the activation of the OMA-1 protein, which regulates the cutting of OPA-1. OPA-1 has two isoforms: a long (active) and short (inactive) isoforms. Our research is exploring the impact of the levels of OPA1 expression on the observed $\Delta\psi_m$ threshold of mitochondrial fusion. Our laboratory has demonstrated that 143B cells lose L-OPA1 isoforms at [CCCP]> 4.75 μM and AC16 between 2-4μM of CCCP. We have also discovered that endogenous levels of OPA1 are higher in 143B in comparison to the AC16, which may confer heightened sensitivity to loss of $\Delta\psi_m$. To test this, transfection of exogenous OMA1 and OPA1 will be done to monitor the resistance to CCCP treatment.

DEDICATION

The completion of my master's was made possible due to the sacrifice, love and support from my family. My mother, Patricia Schutz constantly inspired me to become better each day through her faith, positivity, and determination. Her perfectionistic mentality has made her the person she is today, and it has guided me through life's ups and downs. My father, Marco Antonio De La Torre has showed me that sacrifice and love are one in the same. His sacrifices motivated me to always give my best in every aspect of my life. He is the true embodiment of a loving and caring father. I am truly grateful to both of them for making me the man I am today. My darling wife, Jessica Maria Jones pushed me and encouraged me since the first day we met. She led by example as she was accepted into medical school thanks to her incredible work ethic. I hope to catch up to her in the near future.

ACKNOWLEDGMENTS

I will be forever grateful to Dr. Robert Gilkerson for everything he's done for me since I joined his laboratory. He has been a life saver from the very beginning as he guided me through my research and encouraged me to push myself and increase my knowledge as a graduate student. Without his help I would not have been able to stay in this country, much less finish my studies. I would also like to thank Dr. Megan Keniry for initially encouraging me to start research and for being such kind and caring professor. Additionally, I would like to thank Dr. Nirakar Sahoo for his guidance and support in building my thesis.

I would also like to thank the administration of the Graduate College at UTRGV for helping me with every question and concern I had throughout my time here as a student.

TABLE OF CONTENTS

LIST OF FIGURES

Page

CHAPTER 1

INTRODUCTION

The mitochondrion is an organelle that is responsible for many processes within the cell. It encompasses the Krebs cycle, β-oxidation, heme biosynthesis, calcium handling and oxidative phosphorylation (Mishra, 2016). Mitochondria are widely known for their crucial responsibility in ATP production. For this to occur, an electrochemical gradient must be formed within the intermembrane space. In the inner membrane, Complexes I through IV transfer electrons from NADH and FADH2 to carry out the proton pumping that establishes the transmembrane potential ($\Delta\psi m$). This electrochemical gradient drives ATP synthesis by the F1F0 ATP synthase (Schon 2018).

The metabolism of cells involves the glycolytic pathway, the Krebs cycle (in animals) and the Calvin cycle (in plants) as well as β-oxidation. These pathways create the byproducts NADH and $FADH_2$. The Krebs cycle within the mitochondrial matrix allows for the high yield of these electron carriers. β-oxidation is also a key pathway in the production of these electron carriers from the degradation of fatty acids.

The Electron Transport Chain (ETC) is responsible for pumping hydrogen ions into the intermembrane space of the mitochondria to form an electrochemical gradient known as the transmembrane potential ($\Delta\psi m$). Complex I receives the electrons from NADH to gain enough energy to pump hydronium ions (H+) to the intermembrane space. The electrons are then

transferred to the intermediate, cytochrome Q (CytQ). FADH2 feeds its electrons into complex II, which relays them to CytQ. Cytochrome Q is then responsible for transferring those electrons to complex III, which will give complex III enough energy to pump hydronium ions into the intermembrane space. Cytochrome c (CytC) then receives the electrons from Complex III and transfers them to Complex IV which once again allows for the pumping of hydronium ions to the intermembrane space. The final electron acceptor of the ETC is oxygen, which receives the electrons and reacts with hydronium ions to create water. This constant pumping of hydronium ions creates the electrochemical gradient between the intermembrane space and the matrix of the mitochondria. The electrochemical gradient allows for the F1F0 ATP synthase to synthesize ATP at large quantities.

Mitochondria are dynamic organelles that maintain an equilibrium between fission and fusion. These dynamic states affect the bioenergetics of the mitochondria in a direct "structure/function" relationship (Jones et al. 2017). The loss of $\Delta\psi m$ impacts the role of oxidative phosphorylation. Hence, leading to a fragmented network that has the potential to lead to apoptosis. Fusion is mediated by a variety of factors, including mitofusins 1 and 2 (MFN1, MFN2) and optic atrophy protein 1 (OPA1) (Schon et al. 2010). Conversely, fission, is promoted by mitochondrial fission protein 1 (FIS1) and dynamin-related protein 1 (DRP1) (Schon et al. 2010). DRP1 is a cytosolic protein that is recruited to the mitochondria for the process of fission. DRP-1 assembles as a multimeric 'collar' that makes a ring-like structure around the mitochondria and pinches it in order to fragment the organelle (Loson et al. 2013). If the dynamic equilibrium of fission and fusion is not maintained, the cell is primed for apoptosis. Defects in the fusion pathway have led to neurodegenerative disease due to unopposed fission of

the mitochondria. Therapeutic treatments have shown potential by "promoting fusion via fission inhibition" with a drug-based approach (Schon et al. 2010).

OPA1 mediates fusion, linking bioenergetic function with structural dynamics. OPA1 is responsible for the fusion of the mitochondria and has 5 protein isoforms (Griparic et al., 2007), produced from 7 mRNA splice variants (Delettre et al., 2001). The functional isoforms of critical importance for mitochondrial fusion are the long isoforms a and b (L-OPA1). In response to cellular stress (including loss of $\Delta\psi m$), OMA1 cleaves the L-OPA1 isoforms turning it into the short isoforms c, d, and e (S-OPA1). When OPA1 is cleaved to short isoforms, mitochondrial fusion is lost. The cleavage of L-OPA1 can cause the cell to be sensitized for apoptosis (Head et al. 2009, Ehses et al. 2009). OMA1 is dependent on membrane potential in order for it to be activated and cleave L-OPA1 (Anand et al. 2014; Rainbolt et al. 2016). The membrane potential of the mitochondria can be disrupted by using carbonyl cyanide m-chlorophenyl hydrazine (CCCP) which will therefore activate OMA1.

Previous research from our laboratory has shown a sharp threshold for the cleavage of L-OPA1 and fusion in 143B osteosarcoma cells: titration of CCCP shows that 143B cells maintain mitochondrial fusion and L-OPA1 isoforms until $\Delta\psi_m < 33\%$ of controls (Jones et al. 2017). Here, we explore $\Delta\psi_m$ -sensitive mitochondrial dynamics in the AC16 cardiomyocyte cell line. Western blot analysis examined the loss of L-OPA1 isoforms at concentrations 2-4μM of CCCP. Immunofluorescence imaging supported this data with images of clear fragmentation of mitochondria. Our data demonstrate that AC16 cardiomyocytes lose mitochondrial fusion at CCCP concentrations greater than 2 μM, representing a distinct difference from 143B osteosarcomas. Strikingly, endogenous OPA1 levels are significantly lower in AC16s than

143Bs, motivating future exploring the impact of OPA1 expression as a major determinant of $\Delta\psi_m$ -sensitive mitochondrial dynamics.

CHAPTER II

METHODOLOGY AND FINDINGS

Materials and Methods

Cell culture: 143B osteosarcoma (kind gift of Dr. Eric Schon, Columbia University) were grown at 37 degrees in 5% CO2 in Dulbecco's Modified Eagle's Medium (DMEM, Gibco) supplemented with 10% fetal bovine serum (FBS) with antibiotic/antimycotic. AC16 cardiomyocytes (ATCC) were grown in F12 media supplemented with 10% fetal bovine serum (FBS) with antibiotic/antimycotic. Carbonyl cyanide 3-chlorophenyl hydrazine (CCCP) was added from a 10 mM stock solution in DMSO, added to media at the indicated concentrations, and incubated for 1 hour.

Immunofluorescence microscopy: Cells were seeded to glass coverslips for immunomicroscopy. The coverslips are then washed twice with 2 milliliters of 1X phosphate-buffered saline (PBS) for 2 minutes each wash. The cells are then fixed by using 2 milliliters of 4% paraformaldehyde for 30 minutes. Once again, the cells are washed twice with 2 milliliters of 1X PBS for 2 minutes each. The cells will then be permeabilized by using 2 milliliters of 0.1% Triton-100 for 10 minutes. The cells are then washed twice with 2 milliliters of 1X PBS for 2 minutes each. The blocking stage then takes one hour after using 100 microliters of 10% normal goat serum (NGS). Immediately after the blocking stage the cells are incubated with one microliter of the TOM20 antibody in 100 microliters of 1X PBS for one hour and thirty minutes.

A set of three consecutive washes with 1X PBS for 5 minutes each follows this step. The cells are then incubated for one hour with the secondary antibody, which is the goat anti-rabbit Alexa Fluor 488. The concentration of the secondary antibody follows that of the primary antibody. There is 1 microliter of the Alexa Flour 488 antibody in 100 microliters of 1X PBS. In order to ensure the proper binding of the secondary and primary antibody a secondary coverslip is placed on top of the coverslip that the cells have attached to. Once the hour is finished the top coverslip is removed and set of three consecutive washes with 2 milliliters of 1XPBS for 5 minutes each, follows the incubation. In order to see the nucleus clearly in the images the cells are incubated with two microliters of DNA-binding DAPI in one milliliter of 1X PBS for 5 minutes. The addition of a second coverslip on top of the primary coverslip is also done in this step. After the DAPI incubation two sets of two-minute washes, with 2 milliliters of 1XPBS are done. A slide is prepared by placing five microliters of 50% glycerol in the middle of the slide. The coverslips are then placed on the slide with the face down. Elmer's cement glue is used on the surroundings of the coverslip to prevent movement in the confocal. A variety of settings have to be adjusted in the confocal before taking an image. The objective lenses should be at 60X magnification with the confocal aperture set at 1. The image is magnified to 3.0x and the image size of 1024x1024 is chosen. Speed and quality should be placed at High Quality (x16). The laser settings for DAPI should be adjusted to 10% or to a setting where the nucleus is visible. The Alexa Fluor 488 laser setting should be set to 40% to maximize the absorbance. Finally, the sensitivity of both the DAPI and the Alexa Fluor 488 should be set to 49.6%. The image is then taken and saved to its respective file. 6% western blot gel preparation: in order to properly run a western blot using the OPA1 protein, one needs to make a 6% separating polyacrylamide gel. The gel has to be made in two layers, the stacking layer and the separating layer. A mixture of the following will be

made:100 microliters of 10% Sodium Dodecyl Sulfate (SDS), 5.3 milliliters of deionized water, 2.5 milliliters of Tris 1.5M base at a pH of 8.8, and 2 milliliters of acrylamide 30% are first mixed in a test tube. Finally, the solidifying step for the mixture of the separating gel involves the addition of both 100 microliters of 10% ammonium persulphate solution (APS) and 8 microliters of tetramethylethylenediamine (TEMED). The final mixture will take 20 minutes to fully solidify. The stacking layer will be a mixture of the following ingredients: 30 microliters of 10% SDS, 1.04 milliliters of deionized water, 375 microliters of Tris 1M base at a pH of 6.8, 510 microliters of 30 % acrylamide. The final step will be mixing two chemicals to solidify this layer. The chemicals included 30 microliters of 10% APS and 3 microliters of TEMED. This layer will solidify in approximately 10 minutes.

Western blotting: 143B and AC16 cells were seeded to 10 cm dishes (Corning) and prepared for Western blotting. Lysates were prepared by removing the media and adding 2 milliliters of cold 1X PBS solution while swirling the dishes for 1 minute. The 1X PBS is removed and a 1 milliliter mixture of 250 microliters of mercaptoethanol and 2.25 milliliters of 2X Laemmli sample buffer are added. The dishes are then swilled on ice for 5 minutes. Cell lifters are then used to scrape the dish to recover all cell samples in a 1.5 milliliter test tube. The test tubes are then placed on a heating block at 99 degrees Fahrenheit for 5 minutes. The test tubes are then centrifuged for 5 minutes and stored in the freezer until further use.

Two main buffers have to be made before running the Western blot. The first is the 1X running buffer which is a mixture of 100 milliliters of 10X running buffer, 10 milliliters of 10% SDS and 890 milliliters of deionized water. The second buffer is the 1X transfer buffer that is made by mixing 100 milliliters of 10X transfer buffer, 100 milliliters of methanol, and 800 milliliters of deionized water. Once the buffers are ready, one can begin to load the wells in the

desired order. For these experiments the first well was loaded with 10 microliters of a protein ladder for reference. From there the experiment followed this loading sequence for the cell lysates: 20 microliters of untreated 143B cells, 20 microliters of 5 micromolar CCCP treated 143B cells, 20 microliters of 10 micromolar CCCP treated 143B cells, 20 microliters of untreated AC16 cells, 20 microliters of 5 micromolar CCCP treated AC16 cells, 20 microliters of 10 micromolar CCCP treated AC16 cells. When the wells are filled one must add the 1X running buffer before starting the electrophoresis. The PowerPac Power supply will be set to 120 volts and it will be set to run the electrophoresis for one hour and thirty minutes. Before the transfer of the gel a PVDF membrane must be cut and briefly washed with methanol and then with transfer buffer. When one is ready to transfer the gel a "sandwich" is created starting with the clear side of the holder the order is as follows: sponge, filter paper wet with transfer buffer, PVDF membrane, polyacrylamide gel, filter paper wet with transfer buffer, and sponge. The sandwich is secured in place and the PowerPac Power supply is set to 120 volts and set to run for one hour. Once the transfer is complete the PVDF membrane is blocked by using 5% milk for one hour. The milk is then briefly washed for 5 minutes with 1X Tris-buffered saline with 0.1% Tween ® 20 Detergent (TBST). The membrane is then incubated with the mouse monoclonal anti-OPA1 antibody overnight. The following day the membrane undergoes two washes with 1X TBST for 7 minutes each. The HRP-antimouse is added at a 3-microliter concentration in 9 milliliters of 1X TBST and it is incubated for one hour. Two washes of 1X TBST follow for 7 minutes each after the incubation. A mixture of 1 milliliter of the detection reagent peroxide solution and 1 milliliter of the detection reagent luminol enhancer solution is added to the membrane for 5 minutes. Primary results are then viewed in the HHMI Kodak machine. The membrane is then washed twice for 5 minutes with 1X TBST. Then it undergoes a second blocking step with 5%

milk for one hour. The alpha tubulin mouse monoclonal is then added at a concentration of 10 microliters in 10 milliliters of 1X TBST, overnight. Two washes of 1X TBST for 7 minutes each follows the primary antibody incubation. The HRP-antimouse antibody is then used in a 3-microliter concentration in 9 milliliters of 1X TBST for 1 hour. After the incubation of the secondary antibody the membrane is washed 2 more times for 7 minutes each with 1X TBST. The mixture of 1 milliliter of peroxide solution and 1 milliliter of luminol enhancer solution is added for 5 minutes before viewing the results in the HHMI Kodak machine.

Results and Discussion

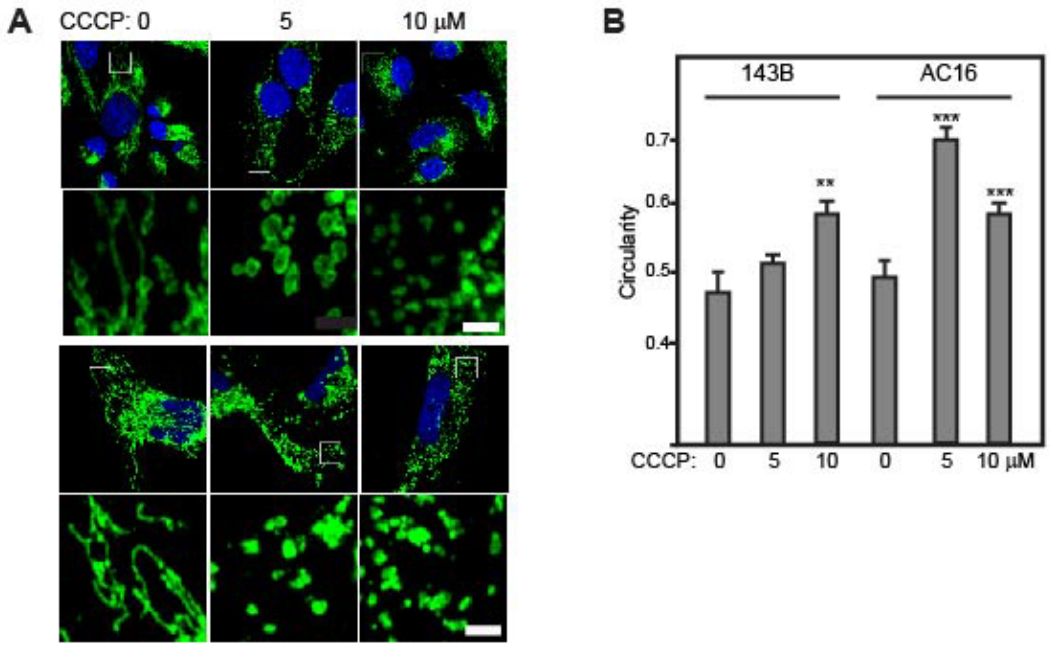

Figure 1. Mitochondria of 143B and AC16 cells fragment under CCCP challenge. A. TOM20 immunofluorescent imaging of 134B osteosarcomas and AC16 cardiomyocytes at 0, 5, and 10 µM CCCP. TOM20 (green) labels mitochondria, DAPI (blue) labels nuclei. Size bar = 2 µM. n=3 expts. B. ImageJ analysis measuring the circularity of the mitochondria in both cell

lines at indicated concentrations of CCCP. n=25 images, +/- standard error. ** denotes $p<0.01$.

AC16 cardiomyocytes fragment more than 143B osteosarcoma cells

AC16 and 143B cells both experience fragmentation of their mitochondria at different concentrations of CCCP. AC16 mitochondria appear to fragment more, in comparison to 143B mitochondria as shown in Figure 1A. The immunofluorescent imaging supports the statement that both cell lines do in fact experience fragmentation of their mitochondria. The graph in Figure 1B. shows that AC16 experience more fragmentation by measuring the circularity of the mitochondria. The graph shows a significant difference between the fragmentation of 143Bs and AC16s at both 5μM of CCCP and 10 μM of CCCP. This increased fragmentation may indicate a heightened sensitivity in the AC16 cell line to stress factors acting on the cell.

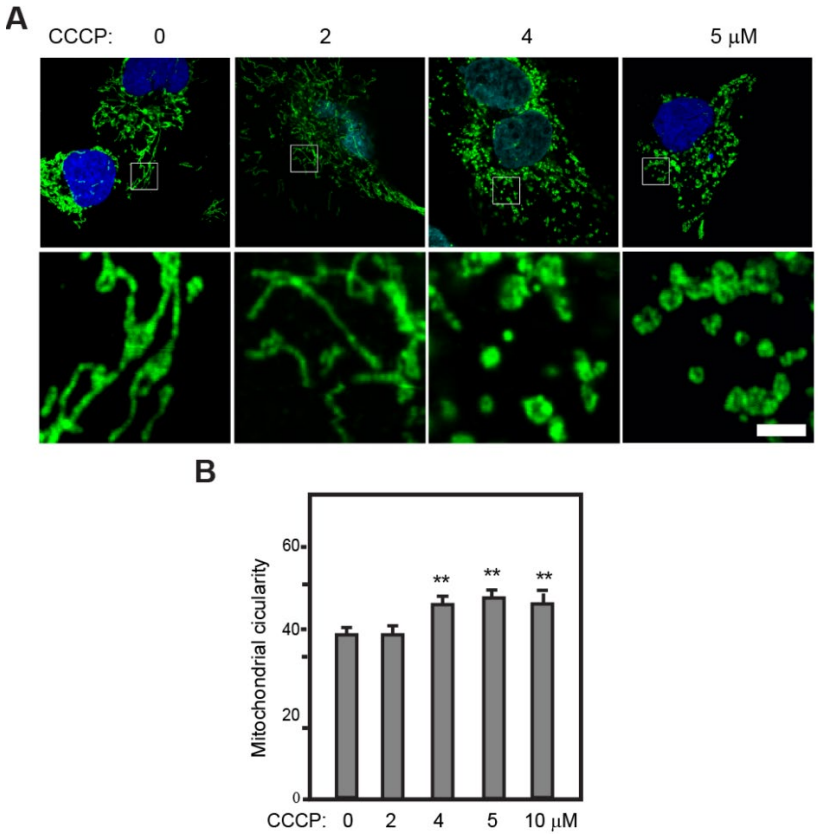

Figure 2. AC16 cells fragment at [CCCP] > 2 uM. A. TOM20 immunofluorescence imaging of AC16s at 0, 2, 4, and 5 μM CCCP. n=3 expts. B. ImageJ analysis measuring circularity of the mitochondria following incubation with CCCP for 1 hr. at 0, 2, 4, and 5 μM. n=25 images +/- standard error. ** denotes $p<0.01$.

AC16 cardiomyocytes lose mitochondrial fusion at [CCCP] > 2 μM

Previously, our laboratory demonstrated that 143B osteosarcoma cells lose mitochondrial fusion at >5 μM CCCP. With the use of immunofluorescence confocal microscopy and western blot analysis, our current results indicate that the AC16 cardiomyocyte cell line loses mitochondrial fusion at > 2 μM CCCP. In Figure 2.A, an antibody against the mitochondrial outer membrane TOM20 protein was used with a goat anti-mouse secondary conjugated with AlexaFluor 488 dye (green) was used to show the

mitochondria of the AC16s. DAPI staining (blue) allowed us to visualize the nuclei of the cells. AC16 cardiomyocytes were incubated at different concentrations of CCCP (0, 2, 4, 5, and 10 μM CCCP) for 1 hr., mounted onto microscope slides, and imaged via confocal microscopy. The circularity of the mitochondrial profiles in n=25 high resolution images were then analyzed by using ImageJ in Figure 2B. A perfect circle would display a value of 1, which would indicate that the mitochondria were fully fragmented. A value closer to 0 would indicate that the mitochondria remain in an interconnected morphology. The results of the ImageJ analysis showed a significant increase in the circularity of the AC16 mitochondria after crossing the 2 μM threshold: at 2 mM, the average mitochondrial circularity was X+/-Y, while at 4 mM CCCP, mitochondrial circularity was Y+/-Z. This change in circularity was maintained throughout the 5 and 10 μM of CCCP concentrations, indicating that the mitochondrial fragmentation had increased in the cell.These results were qualitatively supported by the immunofluorescent images at each concentration, which showed the mitochondria display a fragmented morphology past the 2 μM threshold.

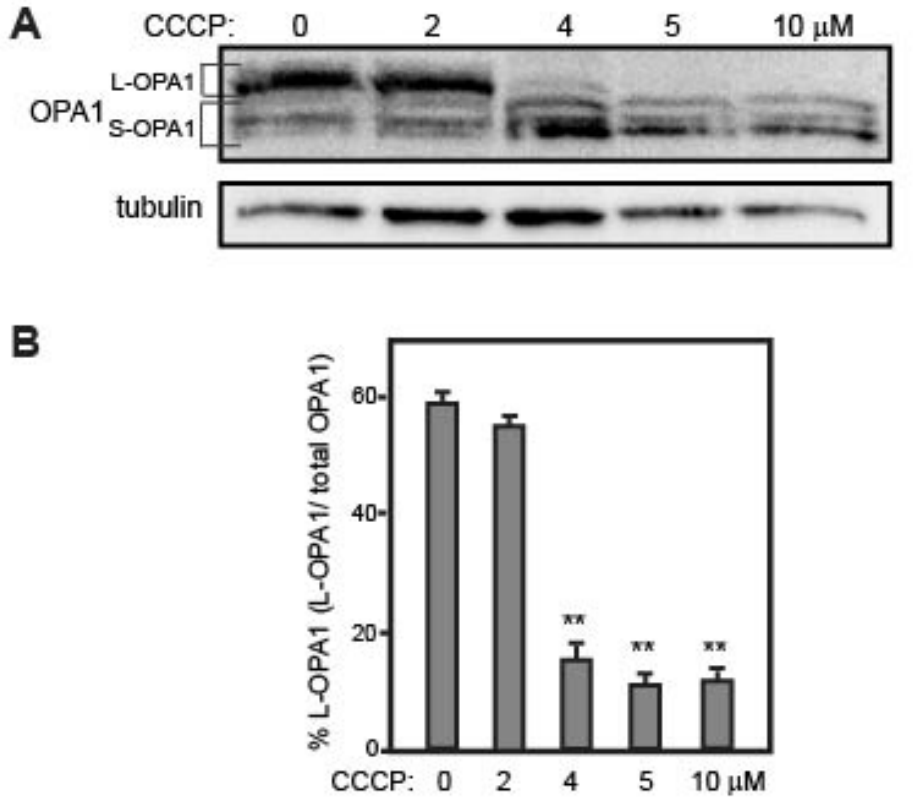

Figure 3. AC16 cells lose L-OPA1 isoforms at [CCCP] > 2 μM. A. Western blot analysis of OPA1 isoforms (top panel) and tubulin (bottom panel, loading control). n=3 expts. Long (L-OPA1) and short (S-OPA1) isoforms of OPA1 are indicated. B. ImageJ analysis of the percent of L-OPA1 out of the total OPA1 signal from Western blot, +/- standard error. ** denotes $p<0.01$. There is a significant decrease in the L-OPA1 concentration > 2 μM.

AC16 cardiomyocytes lose long form of OPA1 (L-OPA1) at [CCCP] > 2 μM threshold.

To examine whether the loss of mitochondrial fusion in AC16s is paralleled by OPA1 status, we conducted Western blot analysis of OPA1 protein under the same conditions, as shown in Figure 3A. While L-OPA1 isoforms were clearly evident at 0 and 2 μM CCCP, the bands corresponding to the L-OPA1 isoforms disappeared at the higher concentrations of CCCP (4,5, and 10). The increased intensity of the band that depicts the short isoform of OPA1 (S-

OPA1) correlates with the disappearance of the L-OPA1 isoform. This may be due to the fact that the L-OPA1 isoforms are cleaved by the OMA1 protease, causing the accumulation of S-OPA1 isoforms. These results suggest that the OMA1 protease is activated by the proportional loss of transmembrane potential (Δψm) at the 2 μM CCCP mark. Tubulin was used as a loading control in all of the lanes for this experiment. The concentration of the L-OPA1 isoform over the total OPA1 concentration was quantified in Figure 3B. This figure correlates with the information in Figure 3A., suggesting that the concentration of the L-OPA1 isoform decreases significantly after the 2 μM threshold.

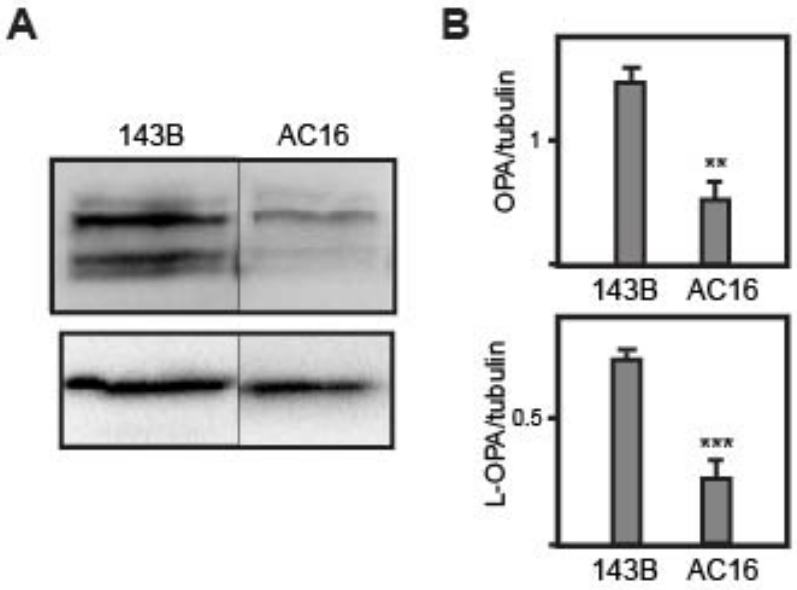

Figure 4. AC16 cells have lower endogenous OPA1 levels than 143B cells. A. OPA1 Western blotting (top panel) of both 143B osteosarcomas and AC16 cardiomyocytes, with tubulin loading control (bottom panel), n=3 expts. B (top graph). ImageJ analysis showing the concentrations of OPA1 protein in both 143B osteosarcomasand AC16 cardiomyocytes. B (bottom graph) shows ImageJ analysis of the concentration of the long isoform of OPA1 (L-OPA1) in both 143B osteosarcomas and AC16 cardiomyocytes. n=3 expts +/- standard error, ** denotes $p<0.01$

AC16 cardiomyocytes show a lower inherent OPA1 concentration in comparison to 143B osteosarcomas.

Figure 4A. shows the western blot analysis and quantifications of OPA1 in AC16 and 134Bs. There was a significantly lower concentration of OPA1 protein in the AC16s in comparison to the 143Bs. The difference in intensity of the OPA1 bands on the western blot show that AC16 have a lesser concentration of the protein. Figure 4B. (top graph) shows the ImageJ analysis of the total concentration of OPA1 in both cell lines. The quantification of the OPA1 proteins correlates with the results form Figure 4A.in that there is a significantly lower concentration of OPA1 protein in the AC16s. Figure 4B. shows the quantification of the long isoform of OPA1 in both 143Bs and AC16s through ImageJ analysis. The results correlate with both Figure 4A and Figure 4B. showing that AC16s have a significantly lower concentration of the long isoform of OPA1. This may explain the reason behind the increased sensitivity to CCCP in the AC16 mitochondria.

CHAPTER III

SUMMARY AND CONCLUSION

Here, we investigate $\Delta\psi_m$ -sensitive mitochondrial fusion in AC16 cardiomyocytes. AC16 cardiomyocytes show an increased sensitivity to CCCP-induced mitochondrial fragmentation, compared with 143B osteosarcoma cells. This was shown through immunofluorescent imaging and western blot analysis. The lower levels of the endogenous OPA1 protein may correlate with the heightened sensitivity of AC16s to loss of $\Delta\psi_m$ as induced by CCCP treatment. This is consistent with a role for OPA1 expression as the major mechanism that determines $\Delta\psi_m$ -sensitive mitochondrial morphology in the AC16 cells. We therefore hypothesize that increasing OPA1 expression will 'shift' the threshold, increasing the ability of AC16 cells to maintain mitochondrial fusion under CCCP challenge, while increased expression of OMA1 will sensitize AC16 cells to CCCP-induced fragmentation.

Future experiments will explore this hypothesis in our experimental system using exogenous expression constructs, directly testing whether OPA1 and OMA1 expression levels correlate with the transmembrane potential threshold of the AC16s. OPA1 and OMA1 transfections will be run to visualize if changes in their expression will be able to shift the threshold of mitochondrial fusion. Side-by-side analysis of AC16s treated with 4 μM CCCP without or with exogenous OPA1 transfection will test whether increased OPA1 levels protects against CCCP-induced mitochondrial fragmentation. Similarly, side-by-side challenge of AC16s with 2 μM CCCP without or with exogenous OMA1 transfection will test the impact of OMA1

levels. Liposome-mediated transient transfection (via Lipofectamine 3000) will allow transfection of AC16s with pCMV-Tag4-OMA1 or pMSCV-OPA1 expression constructs (Addgene, in-hand). Both of these experiments will be followed with immunofluorescent imaging and western blot analysis, as above, to visualize the mitochondrial morphology and OPA1/OMA1 expression.

The interaction of OMA1 and OPA1 provides a critical mechanism of mitochondrial structure/function homeostasis, with key impacts on cell-wide pathways including apoptosis and autophagy. As such, these studies provide a novel exploration of a crucial emerging mechanism of cell stress response. The knowledge gained may provide basic scientific knowledge that can motivate rational therapeutic strategies to prevent or ameliorate mitochondrial dysfunction in a wide range of prevalent human pathologies, including cardiac and neurodegenerative diseases. OMA1 attenuation protect against apoptosis in mouse models of both neurodegeneration (Korwitz et al. 2016, J. Cell Biol.) and heart failure (Acin-Perez et al. 2018, Sci. Transl. Med.), providing proof of principle for novel interventions to protect human health.

REFERENCES

Ehses S., Raschke I., Mancuso G., Bernacchia A., Geimer S., Tondera D., Martinou J.-C., Westermann B., Rugarli E.I., Langer T. 2009. Regulation of OPA1 processing and mitochondrial fusion by m-AAA protease isoenzymes and OMA1. J. Cell Biol. 187:1023–1036.

Friedman J.R., Nunnari J. 2014. Mitochondrial form and function. Nature. 505:335–343.

Head B., Griparic L., Amiri M., Gandre-Babbe S., van der Bliek A.M. 2009. Inducible proteolytic inactivation of OPA1 mediated by the OMA1 protease in mammalian cells. J. Cell Biol. 187:959–966.

Jones E., Gaytan N., Garcia I., Herrera A., Ramos M., Agarwala D., Rana M., Innis-Whitehouse W., Schuenzel E., Gilkerson R. 2017. A threshold of transmembrane potential is required for mitochondrial dynamic balance mediated by DRP1 and OMA1. Cell. Mol. Life Sci. 74:1347–1363.

Loson O.C., Song Z., Chen H., Chan D.C. 2013. Fis1, Mff, MiD49, and MiD51 mediate Drp1 recruitment in mitochondrial fission. Mol. Biol. Cell. 24:659–667.

Schon E.A. 2018. Bioenergetics through thick and thin. Science. 362:1114–1115

Griparic, L., Kanazawa, T., & van der Bliek, A. M. (2007). Regulation of the mitochondrial dynamin-like protein Opa1 by proteolytic cleavage. The Journal of cell biology, 178(5), 757–764. https://doi.org/10.1083/jcb.200704112

Delettre, C., Griffoin, J. M., Kaplan, J., Dollfus, H., Lorenz, B., Faivre, L., ... & Hamel, C. P. (2001). Mutation spectrum and splicing variants in the OPA1 gene. Human genetics, 109(6), 584-591.

Anand, R., Wai, T., Baker, M. J., Kladt, N., Schauss, A. C., Rugarli, E., & Langer, T. (2014). The i-AAA protease YME1L and OMA1 cleave OPA1 to balance mitochondrial fusion and fission. Journal of Cell Biology, 204(6), 919-929.

Rainbolt, T. K., Lebeau, J., Puchades, C., & Wiseman, R. L. (2016). Reciprocal Degradation of YME1L and OMA1 Adapts Mitochondrial Proteolytic Activity during Stress. Cell reports, 14(9), 2041–2049. https://doi.org/10.1016/j.celrep.2016.02.011

Korwitz, A., Merkwirth, C., Richter-Dennerlein, R., Tröder, S. E., Sprenger, H. G., Quirós, P. M., López-Otín, C., Rugarli, E. I., & Langer, T. (2016). Loss of OMA1 delays neurodegeneration by preventing stress-induced OPA1 processing in mitochondria. The Journal of cell biology, 212(2), 157–166. https://doi.org/10.1083/jcb.201507022

Acin-Perez, R., Lechuga-Vieco, A. V., Del Mar Muñoz, M., Nieto-Arellano, R., Torroja, C., Sánchez-Cabo, F., Jiménez, C., González-Guerra, A., Carrascoso, I., Benincá, C., Quiros, P. M., López-Otín, C., Castellano, J. M., Ruíz-Cabello, J., Jiménez-Borreguero, L. J., & Enríquez, J. A. (2018). Ablation of the stress protease OMA1 protects against heart failure in mice. Science translational medicine, 10(434), eaan4935. https://doi.org/10.1126/scitranslmed.aan4935

BIOGRAPHICAL SKETCH

Patrick De La Torre Schutz completed his Bachelor of Science in Biology, with a minor in Chemistry at The University of Texas Rio Grande Valley Spring of 2019 and was awarded a Master of Science in Biology from the University of Texas Rio Grande Valley in May 2021.

Contact information, e-mail: patrickdelatorre23@outlook.com